Received: 17 February 2021 | Revised: 7 April 2021 | Accepted: 21 April 2021

DOI: 10.1111/jace.17878

Journal of the American Ceramic Society

ORIGINAL ARTICLE

Dielectric resonator antenna with $Y_3Al_5O_{12}$ transparent dielectric ceramics for 5G millimeter-wave applications

Chao Du[1] | **Mao-Sen Fu**[2] | **Di Zhou**[1] | **Huan-Huan Guo**[1] | **He-Tuo Chen**[3,4] | **Jian Zhang**[3,4] | **Jun-Ping Wang**[3,4] | **Shao-Fei Wang**[5] | **Hai-Wen Liu**[5] | **Wen-Feng Liu**[6] | **Long Li**[7] | **Zhuo Xu**[1]

[1]Electronic Materials Research Laboratory, Key Laboratory of the Ministry of Education and International Center for Dielectric Research, School of Electronic Science and Engineering, Xi'an Jiaotong University, Xi'an, China

[2]Shaanxi Materials Analysis and Research Center, School of Materials Science and Engineering, Northwestern Polytechnical University, Xi'an, China

[3]State Key Laboratory of High Performance Ceramics and Superfine Microstructure, Shanghai Institute of Ceramics, Chinese Academy of Sciences, Shanghai, China

[4]CAS Key Laboratory of Transparent Opto-functional Inorganic Materials, Shanghai Institute of Ceramics, Chinese Academy of Sciences, Shanghai, China

[5]School of Electronic and Information Engineering, Xi'an Jiaotong University, Xi'an, China

[6]State Key Laboratory of Electrical Insulation and Power Equipment, Xi'an Jiaotong University, Xi'an, China

[7]School of Electronic Engineering and the Collaborative Innovation Center of Information Sensing and Understanding, Xidian University, Xi'an, China

Correspondence
Di Zhou, Electronic Materials Research Laboratory, Key Laboratory of the Ministry of Education and International Center for Dielectric Research, School of Electronic Science and Engineering, Xi'an Jiaotong University, Xi'an, China.
Email: zhoudi1220@gmail.com

He-Tuo Chen, State Key Laboratory of High Performance Ceramics and Superfine Microstructure, Shanghai Institute of Ceramics, Chinese Academy of Sciences, Shanghai, China.
Email: chenhetuo@mail.sic.ac.cn

Funding information
State Key Laboratory of Electrical Insulation and Power Equipment, Grant/Award Number: EIPE19210; National Key Research and Development Program of China, Grant/Award Number: 2017YFB0406301; Fundamental Research Funds for the Central Universities, Grant/Award Number: xzy022020046; Natural Science Foundation of Shanghai, Grant/Award Number: 19ZR1465000

Abstract

Microwave dielectric ceramics are considered to be one of the key materials for dielectric resonators (DR) and have very broad application prospects in the fifth generation (5G) mobile communication system. Here we have prepared high-quality factor $Y_3Al_5O_{12}$ (YAG) transparent dielectric ceramics using high-purity α-Al_2O_3 and Y_2O_3 powders by cold isostatic pressing of the vacuum sintered with tungsten meshes as the heating elements. Optimum relative permittivity (ε_r) ~10.53, quality factor $Q \times f$ (Q = 1/dielectric loss, f = resonant frequency) ~95, 270 GHz (at =7.37 GHz), and temperature coefficient of resonant frequency (TCF) ~ −51.7 ppm $°C^{-1}$ were obtained at a sintering temperature of 1780°C for 12 h. For the first time, YAG transparent ceramic dielectric resonator antenna (DRA) is designed as a dominant TE^{y}_{111} mode and a higher-order TE^{y}_{113} mode using the aperture coupling feeding configuration excitation. The proposed transparent dielectric ceramic DRA can provide a broad impedance bandwidth of 4.193 GHz (ranging from 21.90 to 26.09 GHz) for $S_{11} < -10$ dB, radiation efficiency of 92.1%, and compact DR unit. The proposed DRA can be used potentially as a 5G millimeter (mm)-wave multiple-input-multiple-output (MIMO) antenna unit.

KEYWORDS

5G millimeter-wave applications, dielectric resonator antennas, microwave dielectric properties, transparent ceramics

1 | INTRODUCTION

With the rapid development of mobile data request, it is necessary of the fifth generation (5G) mobile network to tremendously increase communication capacity utilizing not only the extensive amount of spectrum in the millimeter-wave (mm-wave) band[1,2] but also the large-scale multiple-input-multiple-output (MIMO) antenna systems.[3,4] The MIMO technology is capable of improving the communication quality and increasing the channel capacity of a communication system by multiple antennas at both transmitter and receiver sides.[5] Thus, MIMO technology becomes an effective technology in 5G mm-wave applications.[6] However, in the massive MIMO systems, the miniaturization, lightweight, and high performance of the antenna elements will be needed urgently.

In recent years, researchers have worked on the design of dielectric resonator antenna (DRA) for MIMO antennas in the microwave and millimeter wave range,[7,8] as DRA offers several advantages over microstrip patch antennas like wider bandwidth, higher gain and efficiency, and easier excitation.[9] In addition, DRA is made purely of dielectric, so even in the mm-wave frequency band, its loss can be kept at an extremely low level. All of these properties make DRA an excellent antenna candidate for mm-wave applications.[10] Recently, some reported articles mainly concentrate on DR-based 5G mm-wave antennas for decoupling, wideband, and array applications.[7,11,12] However, most of the DR materials applied in these antennas use a mechanical mixture of organic polymer and ceramic powder, which is difficult to ensure its isotropy. Besides, the dielectric loss of DR is commonly not well considered, which will reduce the radiation efficiency of the antenna element and increase the design complexity of the MIMO system.

At present, the microwave dielectric ceramic DRA has the advantages of small size, light weight, and high-quality factor (Q) and offers wide application prospects in the 5G market, so that it is gradually becoming the mainstream of 5G mm-wave applications.[13] Electromagnetic resonance occurs within the ceramic dielectric material, so that higher demands are placed on the performance of dielectric microwave ceramic materials: (a) Suitable dielectric constant (ε_r). High dielectric constant can make the size of the device miniaturized, but too much dielectric constant increases the transmission loss. Therefore, it is necessary to consider the design requirements of the device in order to select an appropriate dielectric constant. (b) High Q. The higher the Q, the smaller the dielectric loss of the DRA, which can achieve better antenna radiation performance. Yttrium Aluminum Garnet ($Y_3Al_5O_{12}$, YAG) transparent ceramics are potential candidates for 5G mm-wave applications due to their excellent properties, such as suitable dielectric constant, low dielectric loss, corrosion resistance, high-temperature stability, and high transparency.[14–16] Usually, two raw material powders Y_2O_3 and Al_2O_3 are mixed to prepare YAG transparent dielectric ceramics through solid-state reaction sintering.[17–20] And solid-state reaction sintering is a relatively simple method of making transparent YAG dielectric ceramics, and by changing the amount of reactant powder during the dispensing process, it is easy to achieve a range of compositions.[21,22] Finally, YAG powder with high sinter ability can be produced by vacuum sintering to produce a fully dense and transparent dielectric ceramic.[23] Until now, however, YAG transparent dielectric ceramic has been viewed as one of the challenging raw materials for laser processing in military applications.[24,25] If YAG transparent dielectric ceramics with these excellent properties can be applied to 5G millimeter wave MIMO systems, the antenna elements can achieve miniaturization, light weight, and excellent radiation performance.

In this work, YAG transparent ceramics were produced by vacuum sintering with cold isostatic pressing (CIP) using tungsten fabric as a heating element. We investigated the microstructure, phase structure, transparency, and microwave dielectric properties of YAG transparent ceramics. Then the YAG transparent microwave ceramic is designed as a 5G mm-wave rectangular DRA element of the MIMO antenna, which is fed through the aperture coupling structure. Nevertheless, the dimensions of the DRA must be as large as possible for easier fabrication. In addition, in the millimeter wave frequency band, the fabrication tolerance of the DRA must be as accommodating as possible to minimize the effects of fabrication error. The time domain finite element simulation software CST Microwave Studio2019® is used to simulate the performance of the proposed DRA and process the model according to the optimized size. Finally, the radiant performances of the rectangular DRA element were measured in an anechoic chamber of mm-wave, including the reflection coefficient, radiation pattern and gain. The results of simulation agree well with the measurement (Figure 1).

2 | RESULTS

Crystal structure was examined by X-ray diffraction (XRD) analysis as shown in Figure 2A. XRD pattern of YAG transparent ceramics showed that α-Al_2O_3 and Y_2O_3 were used as raw materials for production. After sintering for 12 h at 1780°C, they were tempered for 10 h at 1450°C and finally had cubic garnet structure.[26] All peaks were marked as spinel phase (JCPDS: 01-071-0255), the figure shows that there is no secondary phase. After mirror polishing, the YAG transparent ceramic samples were thermally etched to observe the microstructure and grain boundaries of the crystal grains by scanning electron microscope (SEM) photographs. Figure 2B shows that the sintered body has a uniform microstructure,

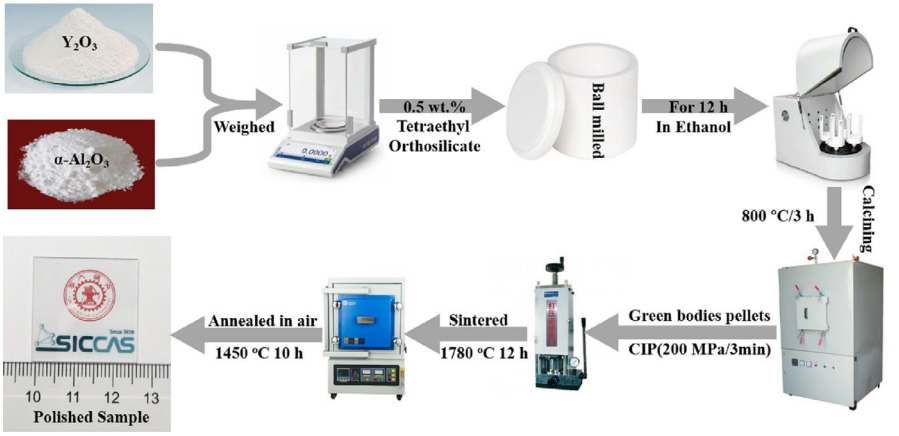

FIGURE 1 The schematic diagrams of experimental preparation processes of the YAG transparent microwave dielectric ceramics [Color figure can be viewed at wileyonlinelibrary.com]

and there are no pores and impurities in or between the grains, and the average grain size is 0.059 mm. At the same time, YAG transparent ceramics have high transparency at wavelengths ranging from the ultraviolet to the midinfrared, which can be applied to a decorative antenna or a transparent multifunctional antenna; it will make the DRAs resonator material more abundant and more choice. In Figure 2C it can be seen that the transmission curve of the YAG transparent ceramics sample with a thickness of 1.02 mm is transparent in the wavelength range from 0.2 to 6.5 μm and the transmission in the range from 0.35 to 5.5 μm 82% can reach. Table 1 shows the dielectric properties of YAG transparent ceramics and corresponding microwave ceramics. The YAG transparent ceramics not only has a good microwave dielectric properties with a relative permittivity ~10.53, a $Q \times f$~ 95, 270 @ 7.37 GHz and a TCF ~ −51.7 ppm °C^{-1} but also have a suitable relative permittivity ($\varepsilon_r = 10.53$) and low dielectric loss ($tg\delta = 7.73 \times 10^{-5}$); it is very suitable for use in millimeter wave antennas. In addition, the dielectric properties of the samples were obtained through closed-cavity resonance testing. This method is a common method for testing the dielectric constant and loss tangent of microwave dielectric materials.

To further investigate the inherent dielectric properties of YAG transparent ceramics, we used the classical harmonic oscillator model to analyze the infrared reflection spectrum of the YAG:

$$\varepsilon^*(\omega) - \varepsilon(\infty) = \sum_{j=1}^{n} \frac{(z_j e)^2 / m_j V_j \varepsilon_0}{\omega_{Tj}^2 - \omega^2 - j\gamma_j \omega} \tag{1}$$

The understanding of the relevant terms in the formula (1) is described in detail in the literature.[27] The relationship between the complex reflectivity $R(\omega)$ and the dielectric constant can be expressed as follows:

$$R(\omega) = \left| \frac{1 - \sqrt{\varepsilon^*(\omega)}}{1 + \sqrt{\varepsilon^*(\omega)}} \right|^2 \tag{2}$$

The infrared reflection spectrum of YAG transparent ceramics can be analyzed in sixteen modes. Table 2 shows the

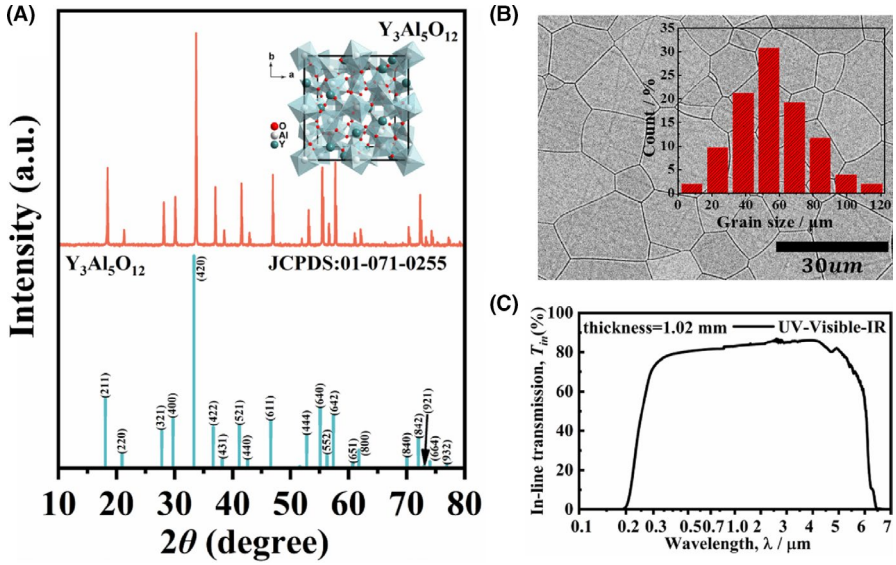

FIGURE 2 (A) X-ray diffraction (XRD) pattern of YAG transparent ceramics sintered at 1780°C (the inset is the crystal structure of YAG) and SEM image (B) (the inset is a schematic diagram of the grain size of YAG). (C) In-line transmittance of YAG transparent ceramics at ultraviolet, visible, and infrared wavelengths [Color figure can be viewed at wileyonlinelibrary.com]

TABLE 1 Comparison of the performance of YAG transparent ceramics and other dielectric ceramics with similar dielectric properties

Sample	T_s (°C)	ε_r	$Q \times f$ (GHz)	f (GHz)	$tan\delta$	TCF (ppm °C^{-1})	References
$Y_3Al_5O_{12}$	1780	10.53	95,270	7.37	7.73×10^{-5}	−51.7	This work
$CaWO_4$	1150	10.40	63,000	10.0	1.5×10^{-4}	−24.4	[36]
$ZnAl_2O_4$-TiO_2	1380	10.30	79,800	11.17	1.4×10^{-4}	−21.5	[37]
$MgAl_2O_4$-TiO_2	1450	10.70	10,540	7.5	7×10^{-4}	−12	[38]
$CaGe_2O_5$	1180	10.90	39,000	10.0	2.5×10^{-4}	NA	[39]

Abbreviation: TCF, temperature coefficient of resonant frequency.

TABLE 2 Phonon parameters of YAG transparent ceramics were determined by fitting the infrared reflection spectrum

Mode	ω_{oj}	ω_{pj}	γ_j	$\Delta\varepsilon_j$
1	156.67	337.65	96.73	4.64
2	164.21	238.62	1.03	2.11
3	218.54	211.25	3.90	0.93
4	266.51	408.17	41.10	2.35
5	286.84	248.22	5.03	0.75
6	323.34	363.38	9.02	1.26
7	367.06	423.39	16.53	1.33
8	389.40	231.99	8.37	0.36
9	423.29	399.30	16.01	0.89
10	446.79	265.06	10.41	0.35
11	510.17	95.64	9.01	0.03
12	564.00	124.94	9.24	0.05
13	688.30	384.33	22.46	0.31
14	724.93	334.02	24.18	0.21
15	786.55	213.19	12.72	0.07
16	798.00	183.63	40.38	0.05

YAG transparent ceramics, $\varepsilon_\infty = 3.54$, $\varepsilon_0 = 10.52$.

relevant phonon parameters of YAG transparent ceramics as representative data. Based on group theory prediction, it has $17A_u + 19B_u$ infrared activation modes. Therefore, the number of fitted modes is less than the theoretical calculation modes. Figure 3A shows the fitted infrared reflection spectrum and the complex relative permittivity. The calculated real part of the relative permittivity of YAG transparent ceramic is 10.53. In addition, it can be observed that the values tested by $TE_{01\delta}$ almost agree with the real and imaginary parts of the calculated relative permittivity. This shows that in the microwave frequency band, the dielectric polarization of YAG is mainly caused by the absorption of phonons in the infrared region.

For the YAG transparent ceramics, we suggest rectangular broadband DRA element for 5G mm-wave applications. Figure 3B shows the geometry of the proposed linear polarization DRA element which fed by an aperture coupling structure, the feed structure consisting of a coupling slot in the ground plane, and a microstrip line opposite the ground plane composition. The length of YAG DR ($\varepsilon_{r,DR}$ =10.53; $tan\delta = 7.73 \times 10^{-5}$) is a and its width d, and the bottom is tightly connected to the slot etched in the center of the grounded Rogers RT5880 substrate ($\varepsilon_{r,DR}$ =2.2; $tan\delta$ = 0.0009) with a thickness of g. The width of the microstrip line is *wf*, the length of the slot is w_s, and the width is l_s. *L* is defined as the side length of the substrate and L_m is the short length of the microstrip line outside the slot. The microstrip line extends to the edge of the substrate where a 50 Ω wave port is used for excitation.[28] On this basis, the antenna element was designed and optimized in CST,[29] and Table 3 contains the design parameters of the proposed antenna.

3 | DISCUSSION

In this section, the operating mechanism of the proposed the rectangular broad-band DRA is investigated. Figure 3B shows the configuration of the aperture coupling rectangular DRA, with the designed resonance frequencies being 22.58 and 25.0 GHz. The slot along the *y*-direction is placed beneath the DRA centrally. It is worth noting that the reason for using the microstrip feedline here is very simple as it is easy to design and manufacture. By using image theory, an isolated rectangular dielectric resonator with a height of 2d is analyzed. The dielectric waveguide model (DWM)[30] can be conveniently used to find the resonance frequencies of various rectangular DRA modes. In this model, the modes of the rectangular dielectric waveguide can be divided into two modes, TM^y_{mnl} and TE^y_{mnl}, where *m*, *n*, and *l* represent the number of extremes in the *x*, *y* and *z* directions, respectively.[11] The TE^y_{111} mode corresponding to the fundamental resonance frequency of the rectangular DRA is defined as follows:

$$f_{DRA} = \frac{c}{2\pi\sqrt{\varepsilon_r}}\sqrt{k_x^2 + k_y^2 + k_z^2} \tag{3}$$

$$k_y = \frac{\pi}{b} = \frac{\pi}{a},\ k_z = \frac{\pi}{2d} \tag{4}$$

$$\tan\left(\frac{ak_x}{2}\right) = \left(\frac{k_{xa}}{k_x}\right),\ k_{xa} = \sqrt{k_x^2 + k_z^2} \tag{5}$$

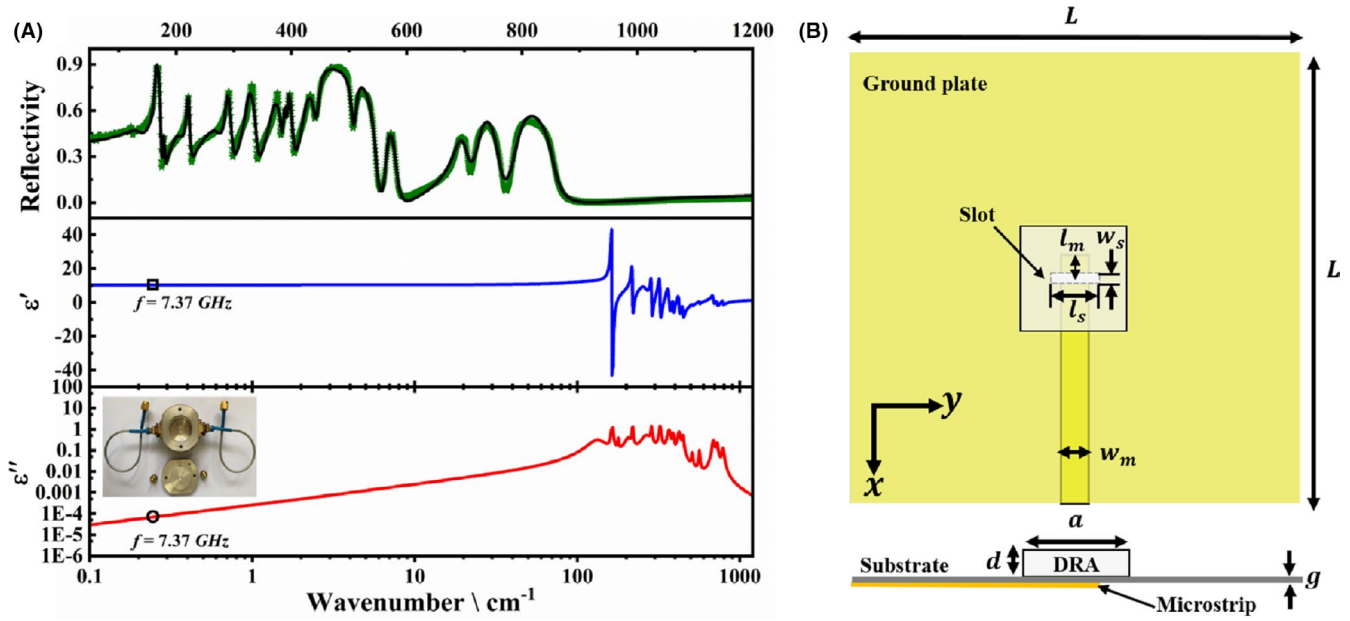

FIGURE 3 (A) The experimental and fitted infrared reflectance spectrum curves of YAG (the black solid line is the fitted, the red circle is the experiment) and the YAG fitted complex dielectric spectrum curve (the square and circular numerical points are measured by closed cavity resonance in the microwave value). (B) Schematic diagram of rectangular dielectric resonator antenna (DRA) structure [Color figure can be viewed at wileyonlinelibrary.com]

TABLE 3 Design the specific parameters of the optimized rectangular DRA

Parameter name	Parameter name	Value (mm)
R-DRA side	a	5.20
R-DRA height	d	1.06
Substrate thickness	g	0.254
Substrate length	L	22.6
Slot width	w_s	0.31
Slot length	l_s	2.05
Microstrip feed width	w_m	1.23
GP side length	l_m	1.25

Abbreviation: DRA, dielectric resonator antenna.

where k_x, k_y, and k_z are wave-numbers along the x-, y- and z -directions, respectively. And c is the speed of light.

Figure 4 shows the distribution of the electric field of the DRA simulated by CST. It can be seen from the figure that the frequency corresponding to the dominant mode TE_{111} is f_1 and the frequency corresponding to the higher-order mode TE_{113} is f_2. It can be found that there is a semicircular electric field in Figure 4B in the internal electric field corresponding to the resonant frequency of mode TE^y_{111} at 22.58 GHz. Due to the mirror effect of the ground plane, a full loop is generated on the z-axis that is equivalent to the TE^y_{111} mode.[31] Meanwhile, the internal E fields of the TE^y_{113} mode at 25.0 GHz,[9] there are the three semicircular electric field in Figure 4D. This figure illustrates that the dominant mode (TE^y_{111}) and high-order mode (TE^y_{111}) of the rectangular YAG transparent ceramic are excited to realize a dual-band broadband antenna element.[32]

Figure 5A shows the antenna measurement setup of the microwave anechoic chamber, and Figure 5C,D exhibits the photograph of the implemented rectangular DRA element. In Figure 5B, the simulated and measured S_{11} results of the proposed YAG transparent ceramic DRA element are compared. The measured bandwidth is 4.19 GHz (ranging from 21.90 to 26.09 GHz) for $S_{11} < -10$ dB, and the simulated bandwidth is 5.04 GHz (ranging from 21.30 to 26.34 GHz) for $S_{11} < -10$ dB. It is obvious that the simulated bandwidth is larger than the measured bandwidth, which can be attributed to the manufacturing deviation of the proposed DRA element. The simulated and measured resonant frequencies at both lower resonant frequency (22.58 GHz) and upper resonant frequency (25.0 GHz) show good agreement, indicating that the YAG transparent ceramic DR are fabricated to be the right dielectric properties.

To demonstrate the radiation performance of the rectangular DRA element, the normalized far-field radiation patterns were simulated and measured at the frequencies of 22.58 and 25.0 GHz in the plane phi=0° and phi=90°, as shown in Figure 6. It can be seen from the figure that the broadside radiation pattern is observed at both resonance frequencies. In the boresight ($\theta = 0°$) direction, the H-plane (x-z plane) and E-plane (y-z plane) copolarized fields are stronger than their cross-polarized counterparts by near 20 and 30 dB,

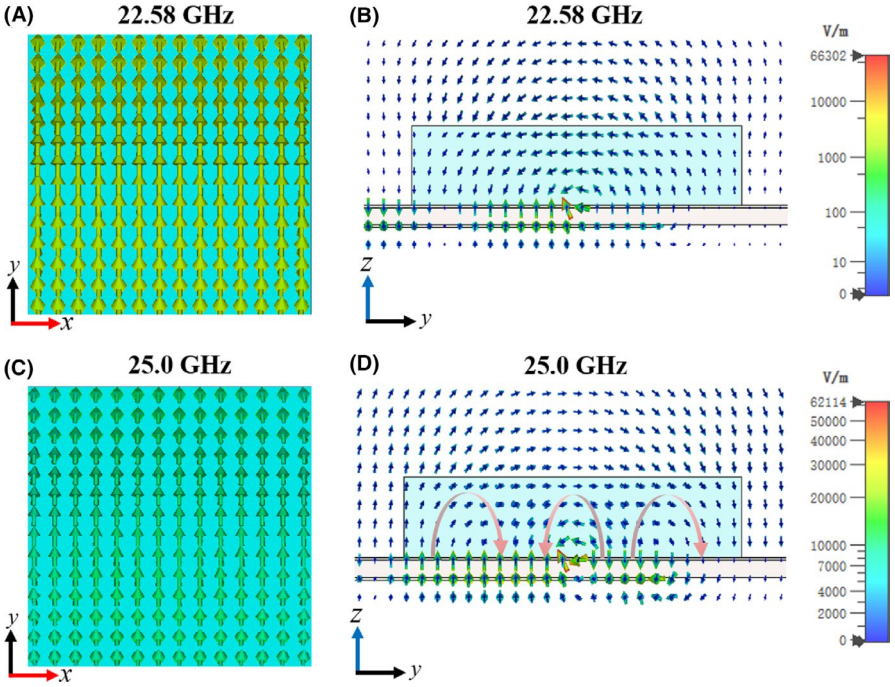

FIGURE 4 *E*-field distribution of TE^{y}_{111} mode at 22.58 GHz: (A) *x y*-plane, (B) *y z*-plane, and TE^{y}_{113} mode at 25.0 GHz: (C) *x y*-plane, (D) *y z*-plane [Color figure can be viewed at wileyonlinelibrary.com]

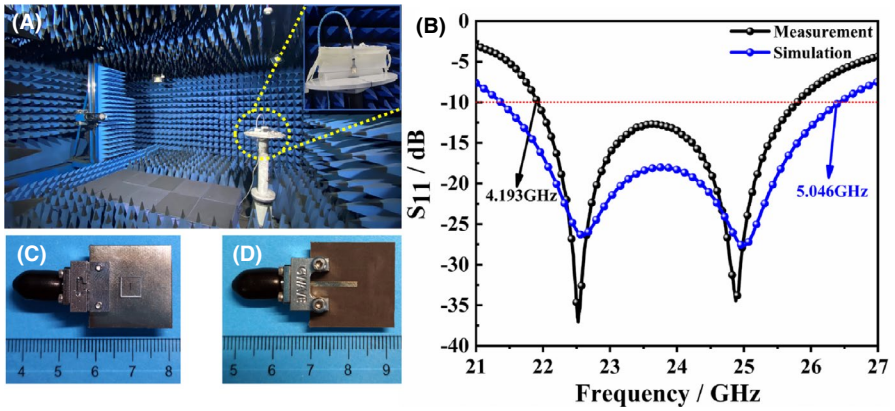

FIGURE 5 (A) The microwave anechoic chamber used for antenna measurement. Prototype of a rectangular DRA: (C) top view, (D) bottom view. (B) Measured and simulated S_{11} results of the proposed rectangular dielectric resonator antenna (DRA) element [Color figure can be viewed at wileyonlinelibrary.com]

respectively. The ripple of the measured pattern is mainly caused by the diffraction of the limited ground plane and the antenna mount.[10] In general, the measurement results of the radiation pattern agree well with the simulation results.

The simulated and measured results of the realized gain of the proposed rectangular YAG transparent ceramic DRA at $\theta = 0°$ and $\varphi = 0°$ are shown in Figure 7. With reference to the figure, the measured realized gain varies between 5.70 and 6.53 dB and the simulated result shows the realized gain variation between 5.78 and 6.86 dB, which is slightly larger than the measurement result. When testing the gain of the antenna, we used the gain-comparison method which the maximum radiation intensity of the antenna under test is compared with the maximum radiation intensity of a standard antenna with known gain by way of comparison, and finally, the gain of the antenna under test is obtained. Therefore, the loss of the cable has been taken into account in the test. Meanwhile, in the simulation, the port used the lossless waveguide port, and in the antenna measurement, a 50 SMA (2.92 mm DC-40 GHz) connector was used. As a result, there is a certain gap between the test and simulation results. At the same time, the simulated radiation efficiency in the entire frequency band exceeds 92.1%. The efficiency is slightly higher than that of conventional DRA.[33,34]

We compared the DR materials of different DRAs for 5G mm-wave applications. As seen from Table 4, we can find that most of the currently reported mm-wave DR materials are generally dielectrics or rogers with high dielectric constant. Due to the loss and dispersion, effect of generally dielectrics DR is much serious in the mm-wave frequency band, which might bring some problems to the design of DRA. Meanwhile, The radiation efficiency of the antenna element is closely related to the $Q \times f$ value of DR materials. However, the YAG transparent ceramics have optimum dielectric loss $\sim 7.73 \times 10^{-5}$, $Q \times f$ (Q = quality factor =1/dielectric loss, f = resonant frequency) ~95, 270 GHz @ 7.37 GHz, which enables the designed DRA element to have high radiation efficiency, and the suitable dielectric constant of YAG transparent ceramics not only can make the size of the device miniaturized but also makes easier

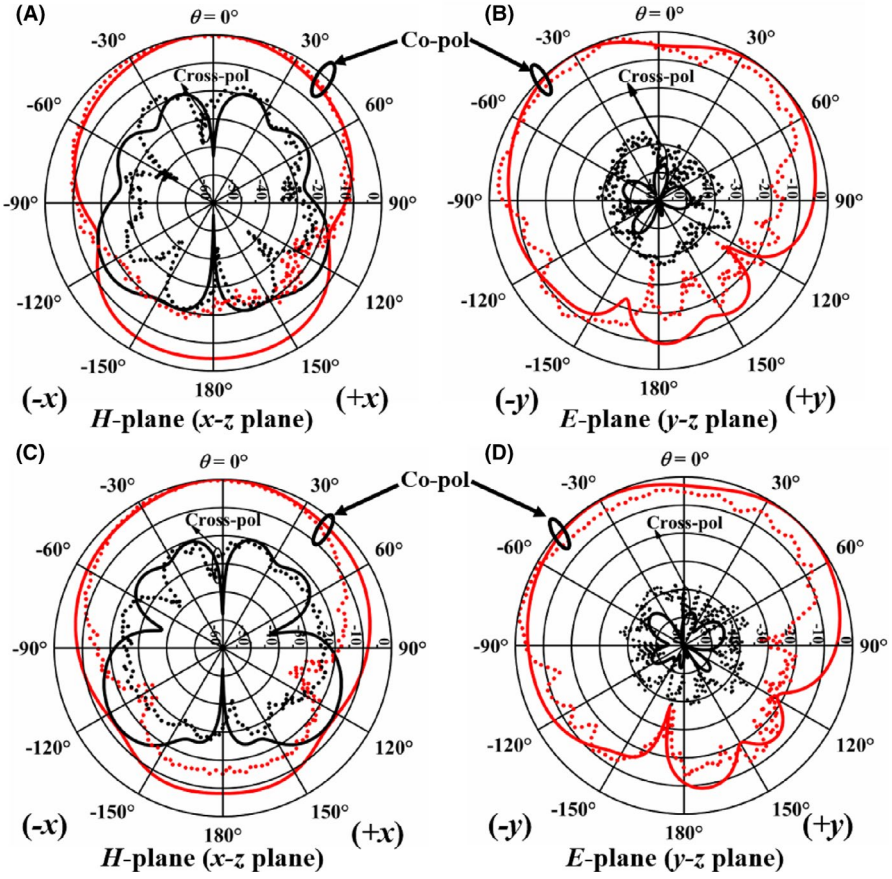

FIGURE 6 Measured (dotted line) and simulated (solid line) normalized radiation patterns of the proposed rectangular dielectric resonator antenna (DRA). (A) *xoy* plane, (B) *yoz* plane of the normalized radiation patterns at 22.58 GHz (TE^{y}_{111}). (C) *xoz* plane, (D) *yoz* plane of the normalized radiation patterns at 25.0 GHz (TE^{y}_{113}) [Color figure can be viewed at wileyonlinelibrary.com]

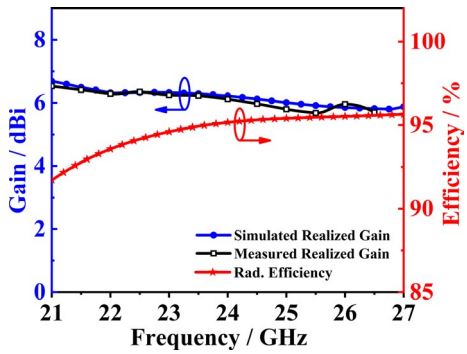

FIGURE 7 Measured (black curve) and simulated (blue curve) gain and simulated radiation efficiency (red curve) of the proposed rectangular dielectric resonator antenna (DRA) element [Color figure can be viewed at wileyonlinelibrary.com]

fabrication. The dielectric constant of YAG transparent ceramics does not change with frequency. Furthermore, the YAG transparent ceramics have consistently high transmittance from ultraviolet to mid-wave infrared, which can be applied to a decorative antenna or a transparent multifunctional antenna; it will make the DRAs resonator material more abundant and more choice. For the above reasons, the YAG transparent ceramics has been chosen the resonator material of the 5G millimeter wave MIMO antenna element.

In this study, the YAG transparent dielectric ceramics were manufactured by CIP using tungsten meshes as a heating element for vacuum sintering. The ceramics sintered at 1780°C have outstanding dielectric properties of $\varepsilon_r \sim 10.53$, $Q \times f \sim 95,270$ GHz and a TCF ~ -51.7 ppm °C^{-1}. Since the YAG transparent ceramic has a suitable relative permittivity, low dielectric loss, and good optical properties, it is becoming a promising material for YAG transparent dielectric ceramic DRA for 5G mm-wave application for the first time. The proposed rectangular broad-band DRA element was excited in its dominant TE^{y}_{111} mode and higher-order TE^{y}_{113} mode using the aperture coupling feed configuration. Measured results show that DRA for $S_{11} < -10$ dB has a broad bandwidth of 4.19 GHz (from 21.90 to 26.09 GHz), and the measured gain varies between 5.70 and 6.53 dB over the entire frequency band. The measurement results are compared with the simulation results, and the results show good agreement. The radiation performance of the proposed DRA shows that it is a good candidate for 5G mm-wave MIMO antenna application.

4 | MATERIALS AND METHODS

4.1 | Sample synthesis

The raw material used for Yttrium Aluminum Garnet ($Y_3Al_5O_{12}$, YAG) is high-purity α-Al_2O_3 powder (purity>99.99%, Aladdin Reagent (Shanghai) Co., Ltd.), Y_2O_3 powder (purity>99.99%, China Yue-long New Material Co.,

DR materials	ε_0	$tg\alpha$	Dispersion	BW (GHz)	References
YAG ceramic	10.53	7.73×10^{-5}	Low	21.90-26.09	This work
Dielectric	5.7	N/A	High	27.70-32.70	[40]
Eccostock hik	10.0	0.002	High	23.30-24.59	[10]
Rogers 6010	10.2	0.002	High	62.70-73.90	[11]
Dielectric	9.8	N/A	High	27.25-28.59	[8]

Abbreviation: DR, dielectric resonator.

TABLE 4 Performance comparison of different DR materials for 5G millimeter-wave applications

Ltd.) used. The starting powder was weighed according to the stoichiometric ratio of YAG and ball-milled for 12 h in an ethanol solution, and 0.5 wt% by weight of tetraethyl-orthosilicate (TEOS, purity>99.99%, Sigma-Aldrich) was added as a sintering additive. The powder mixture was dried at 120°C for 24 h and sieved through a 200-mesh sieve. The organic components were removed by calcination at 800°C for 3 h, and the powder was dry-pressed at 15 MPa. The green pellets were cold isostatically pressed at 200 MPa / 3 min. The compacted pellets were then passed through a vacuum furnace at 1780°C and 10^{-3} Pa and sintered for 12 h with a tungsten wire mesh as a heating element. After vacuum sintering, the sintered precursor was further annealed in air at 1450°C for 10 h. The samples were processed on both sides and optically polished. A schematic diagram of the experimental process is shown in Figure 1.

4.2 | Structural microstructural characterizations and microwave dielectric property

Linear transmittance of transparent ceramics was tested by the Cary-5000 UV-VIS-NIR spectrophotometer produced by the American Varian Company. All the tests were carried out at room temperature. Before testing, samples were polished on both sides. The crystal phases were characterized by XRD (Rigaku D / MAX-2400), where the Cu-Kα radiation (Bruker D2 Phaser) in 2θ is between 5° and 65° and has a step size of 0.02°. A scanning electron microscope (Type: Quanta F250) was used to measure the microstructure of YAG ceramic samples. The infrared reflection spectroscopy was characterized with a Bruker IFS 66v FTIR spectrometer (China, NSRL). The dielectric properties of the microwave are characterized using a microwave network analyzer (HP8720ES, Agilent) using the $TE_{01\delta}$ dielectric resonator method.[35] The TCF was tested with a Delta thermostat (model: Delta 9023, at a temperature of 25°C). The calculation of the TCF (τ_f) is as follows:

$$\mathrm{TCF}\left(\tau_f\right) = \frac{f_{85} - f_{25}}{f_{25} \times (85 - 25)} \times 10^6 \tag{6}$$

where f_{25} and f_{85} are the $TE_{01\delta}$ resonant frequencies at 25°C and 85°C, respectively.

4.3 | Antenna characterizations

The DRA was designed and optimized in the time domain finite element simulation software CST MicrowaveStudio2019®, and the return loss S_{11} of the DRA was tested using a Vector Network Analyzer (VNA) model HP8720ES, Agilent. And before use, the instrument should be calibrated with the antenna test port standard. Furthermore, a 50 Ω SMA (2.92 mm DC-40 GHz) connector is used with the antenna measurement. A radiation pattern defines the variation of the power radiated by an antenna as a function of the direction away from the antenna. The radiation patterns in plane $\varphi = 0°$ and $\varphi = 90°$ were tested microwave anechoic chamber by rotating the antenna method. And we used the gain-comparison method which the maximum radiation intensity of the antenna under test is compared with the maximum radiation intensity of a standard antenna with known gain by way of comparison, and finally, the gain of the antenna under test is obtained. All the above tests were performed in a millimeter-wave far-field anechoic chamber, and the 50 Ω SMA (2.92 mm DC-40 GHz) connector was purchased from Gwave Technology Inc.

ACKNOWLEDGMENTS

This work was supported by the National Key Research and Development Program of China (Grant 2017YFB0406301), the State Key Laboratory of Electrical Insulation and Power Equipment (Grant EIPE19210), the Fundamental Research Funds for the Central Universities (Grant xzy022020046), and the Natural Science Foundation of Shanghai (Grant 19ZR1465000).

CONFLICT OF INTEREST

The authors declare no competing financial interest.

AUTHOR CONTRIBUTIONS

D. Zhou and Z. Xu contributed to the conception of the study; C. Du, H. H. Guo, and H. T. Chen contributed significantly to analysis and manuscript preparation; M. S. Fu, J. Zhang, and J. P. Wang helped perform the analysis with constructive discussions. S. F. Wang, H. W. Liu, W. F. Liu, and L. Li designed the experiments. All authors contributed equally to the writing of the manuscript.

ORCID

Mao-Sen Fu https://orcid.org/0000-0002-3241-5169
Di Zhou https://orcid.org/0000-0001-7411-4658
He-Tuo Chen https://orcid.org/0000-0003-1875-5041

REFERENCES

1. Pi ZY, Khan F. An introduction to millimeter-wave mobile broadband systems. IEEE Commun Mag. 2011;49(6):101–7.
2. Rappaport TS, Shu S, Mayzus R, Hang Z, Azar Y, Wang K, et al. Millimeter wave mobile communications for 5G cellular: it will work. IEEE Access. 2013;1:335–49.
3. Zhang P, Chen J, Yang X, Ma N, Zhang Z. Recent research on massive MIMO propagation channels: a survey. IEEE Commun Mag. 2018;56(12):22–9.
4. Larsson EG, Edfors O, Tufvesson F, Marzetta TL. Massive MIMO for next generation wireless systems. IEEE Commun Mag. 2014;52(2):186–95.
5. Rusek F, Persson D, Buon Kiong L, Larsson EG, Marzetta TL, Tufvesson F. Scaling up MIMO: opportunities and challenges with very large arrays. IEEE Signal Process Mag. 2013;30(1):40–60.
6. Zhou Q, Dai H. Joint antenna selection and link adaptation for MIMO systems. IEEE Trans Veh Technol. 2006;55(1):243–55.
7. Pan YM, Qin X, Sun YX, Zheng SY. A simple decoupling method for 5G millimeter-wave MIMO dielectric resonator antennas. IEEE Trans Antennas Propag. 2019;67(4):2224–34.
8. Zhang Y, Deng J-Y, Li M-J, Sun D, Guo L-X. A MIMO dielectric resonator antenna with improved isolation for 5G mm-wave applications. IEEE Antennas Wirel Propag Lett. 2019;18(4):747–51.
9. Petosa A. Dielectric resonator antenna handbook. Boston: Artech House; 2007.
10. Pan Y-M, Leung KW, Luk K-M. Design of the millimeter-wave rectangular dielectric resonator antenna using a higher-order mode. IEEE Trans Antennas Propag. 2011;59(8):2780–8.
11. Chen Z, Shen C, Liu H, Ye X, Qi L, Yao Y, et al. Millimeter-wave rectangular dielectric resonator antenna array with enlarged DRA dimensions, wideband capability, and high-gain performance. IEEE Trans Antennas Propag. 2020;68(4):3271–6.
12. Sharawi MS, Podilchak SK, Khan MU, Antar YM. Dual-frequency DRA-based MIMO antenna system for wireless access points. IET Microwaves Antennas Propag. 2017;11(8):1174–82.
13. Guo H-H, Zhou D, Du C, Wang P-J, Liu W-F, Pang L-X, et al. Temperature stable $Li_2Ti_{0.75}(Mg_{1/3}Nb_{2/3})_{0.25}O_3$-based microwave dielectric ceramics with low sintering temperature and ultra-low dielectric loss for dielectric resonator antenna applications. J Mater Chem C. 2020;8(14):4690–700.
14. Jiang W, Cheng X, Xiong Z, Ma Z, Ali T, Cai H, et al. Static and dynamic mechanical properties of Yttrium Aluminum Garnet (YAG). Ceram Int. 2019;45(9):12256–63.
15. Krell A, Strassburger E, Hutzler T, Klimke J, Chen W. Single and polycrystalline transparent ceramic armor with different crystal structure. J Am Ceram Soc. 2013;96(9):2718–21.
16. Straßburger E. Ballistic testing of transparent armour ceramics. J Eur Ceram Soc. 2009;29(2):267–73.
17. Li J, Wu Y, Pan Y, Liu W, Huang L, Guo J. Fabrication, microstructure and properties of highly transparent Nd:YAG laser ceramics. Opt Mater. 2008;31(1):6–17.
18. Li X, Li J-G, Xiu Z, Huo D, Sun X. Transparent Nd:YAG ceramics fabricated using nanosized γ-alumina and Yttria powders. J Am Ceram Soc. 2009;92(1):241–4.
19. Li Y, Zhou S, Lin H, Hou X, Li W, Teng H, et al. Fabrication of Nd:YAG transparent ceramics with TEOS, MgO and compound additives as sintering aids. J Alloy Compd. 2010;502(1):225–30.
20. Tang F, Cao Y, Guo W, Chen Y, Huang J, Deng Z, et al. Fabrication and laser behavior of the Yb:YAG ceramic microchips. Opt Mater. 2011;33(8):1278–82.
21. Wu Y, Li J, Pan Y, Guo J, Jiang B, Xu Y, et al. Diode-Pumped Yb:YAG ceramic laser. J Am Ceram Soc. 2007;90(10):3334–7.
22. Zhang W-X, Pan Y-B, Zhou J, Liu W-B, Li J, Jiang B-X, et al. Diode-pumped Tm:YAG Ceramic Laser. J Am Ceram Soc. 2009;92(10):2434–7.
23. Li J, Chen F, Liu W, Zhang W, Wang L, Ba X, et al. Co-precipitation synthesis route to yttrium aluminum garnet (YAG) transparent ceramics. J Eur Ceram Soc. 2012;32(11):2971–9.
24. Maiman TH. Stimulated optical radiation in ruby. Nature. 1960;187(4736):493–4.
25. Maiman TH. Optical and microwave-optical experiments in ruby. Phys Rev Lett. 1960;4(11):564–6.
26. Mane ML, Dhage VN, Shirsath SE, Sundar R, Ranganathan K, Oak SM, et al. Nd:YAG laser irradiation effects on the structural and magnetic properties of polycrystalline cobalt ferrite. J Mol Struct. 2013;1035:27–30.
27. Guo H-H, Zhou D, Pang L-X, Qi Z-M. Microwave dielectric properties of low firing temperature stable scheelite structured (Ca, Bi)(Mo, V)O_4 solid solution ceramics for LTCC applications. J Eur Ceram Soc. 2019;39(7):2365–73.
28. Panda AK, Sahu S, Mishra RK. DRA gain enhancement using a planar metamaterial superstrate. Int J RF Microwave Comput Aided Eng. 2018;28(7):e214451–e214510.
29. Rezaei P, Hakkak M, Forooraghi K. Design of wide-band dielectric resonator antenna with a two-segment structure. Prog Electromagn Res. 2006;66:111–24.
30. Kumar Mongia R, Ittipiboon A. Theoretical and experimental investigations on rectangular dielectric resonator antennas. IEEE Trans Antennas Propag. 1997;45(9):1348–56.
31. Al Salameh MS, Antar YMM, Seguin G. Coplanar-waveguide-fed slot-coupled rectangular dielectric resonator antenna. IEEE Trans Antennas Propag. 2002;50(10):1415–9.
32. Bit-Babik G, Nallo CD, Faraone A. Multimode dielectric resonator antenna of very high permittivity. Antennas Propagation Soc Int Symposium IEEE. 2004;2:1383–6.
33. Chen Z, Wong H, Liu Y. A polarizer integrated dielectric resonator antenna for polarization reconfigurability. IEEE Trans Antennas Propag. 2019;67(4):2723–8.
34. Huang C, Tseng Y. A low-loss dielectric using $CaTiO_3$-modified $Mg_{1.8}Ti_{1.1}O_4$ ceramics for applications in dielectric resonator antenna. IEEE Trans Dielectr Electr Insul. 2014;21(5):2293–300.
35. Krupka J. Frequency domain complex permittivity measurements at microwave frequencies. Meas Sci Technol. 2006;17(6):R55–R70.
36. Kim ES, Chun BS, Freer R, Cernik RJ. Effects of packing fraction and bond valence on microwave dielectric properties of $A^{2+}B^{6+}O_4$ (A^{2+}: Ca, Pb, Ba; B^{6+}: Mo, W) ceramics. J Eur Ceram Soc. 2010;30(7):1731–6.
37. Surendran KP, Santha N, Mohanan P, Sebastian MT. Temperature stable low loss ceramic dielectrics in (1–x)$ZnAl_2O_4$ -xTiO_2 system for microwave substrate applications. Eur Phys J B. 2004;41(3):301–6.
38. Surendran KP, Bijumon PV, Mohanan P, Sebastian MT. (1–x)$MgAl_2O_4$-xTiO_2 dielectrics for microwave and millimeter wave applications. Appl Phys A. 2005;81(4):823–6.

39. Valant M, Suvorov D. Glass-free low-temperature cofired ceramics: calcium germanates, silicates and tellurates. J Eur Ceram Soc. 2004;24(6):1715–9.
40. Baldazzi E, Al-Rawi A, Cicchetti R, Smolders AB, Testa O, Moreno CdJVC, et al. A high-gain dielectric resonator antenna with plastic-based conical horn for millimeter-wave applications. IEEE Antennas Wirel Propag Lett. 2020;19(6):949–53.

How to cite this article: Du C, Fu M-S, Zhou D, et al. Dielectric resonator antenna with $Y_3Al_5O_{12}$ transparent dielectric ceramics for 5G millimeter-wave applications. *J Am Ceram Soc*. 2021;104:4659–4668. https://doi.org/10.1111/jace.17878